An acetylation-mediated chromatin switch governs H3K4 methylation read-write capability

Kanishk Jain[1,2], Matthew R. Marunde[3], Jonathan M. Burg[3], Susan L. Gloor[3], Faith M. Joseph[4], Zachary B. Gillespie[3], Keli L. Rodriguez[3], Sarah A. Howard[3], Irina K. Popova[3], Nathan W. Hall[3], Anup Vaidya[3], Spencer W. Cooke[1], Geoffrey C. Fox[5], Kevin E. W. Namitz[6], Bethany C. Taylor[4], Ellen N. Weinzapfel[3], Marcus A. Cheek[3], Matthew J. Meiners[3], Krzysztof Krajewski[1,2], Michael S. Cosgrove[7], Nicolas L. Young[4], Michael-Christopher Keogh[3*], and Brian D. Strahl[1,2,5,8*]

[1]Department of Biochemistry and Biophysics, University of North Carolina at Chapel Hill, School of Medicine, Chapel Hill, NC;
[2]Lineberger Comprehensive Cancer Center, University of North Carolina at Chapel Hill, School of Medicine, Chapel Hill, NC;
[3]EpiCypher, Inc., Durham, NC;
[4]Verna & Marrs McLean Department of Biochemistry and Molecular Biology, Baylor College of Medicine, Houston, TX;
[5]Curriculum in Genetics and Molecular Biology, University of North Carolina at Chapel Hill, School of Medicine, Chapel Hill, NC
[6]Pennsylvania State University, State College, PA;
[7]Department of Biochemistry and Molecular Biology, Upstate Medical University, Syracuse, NY
[8]Lead Contact
*Correspondence: mkeogh@epicypher.com and brian_strahl@med.unc.edu

KEYWORDS

Chromatin, H3K4 methylation, histone tails, histone acetylation, nucleosomes, readers, writers.

ABSTRACT

In nucleosomes, histone N-terminal tails exist in dynamic equilibrium between free/accessible and collapsed/DNA-bound states. The DNA-bound state is expected to impact histone N-termini availability to the epigenetic machinery. Notably, H3 tail acetylation (*e.g.*, K9ac, K14ac, K18ac) is linked to increased engagement of H3K4me3 by the BPTF PHD finger, but it is unknown if this mechanism has broader extension. Here we show that *cis* H3 tail acetylation promotes nucleosomal accessibility to other H3K4 methyl readers, and importantly, extends to H3K4 writers, notably methyltransferase MLL1. This regulation is nucleosome-dependent and also observed *in vivo*, where H3 acetylation is directly linked to increased levels of H3K4 methylation on the same histone tail. These observations reveal an acetylation 'chromatin switch' on the H3 tail that modulates the accessibility and function of H3K4 methylation in chromatin. Our findings also resolve the long-standing question of why H3K4me3 levels are coupled with H3 acetylation.

INTRODUCTION

In the epigenetic landscape, histone proteins are often variably chemically modified by "writer" enzymes (Jenuwein and Allis, 2001; Strahl and Allis, 2000). Writer-installed post-translational modifications (PTMs) can then be recognized by "reader" proteins and/or removed by "eraser" enzymes. This interplay of PTMs comprises the "histone code," and has a central function in regulating chromatin organization and activity. For example, methylated/acylated lysine or methylated arginine residues of histones can recruit transcription factors to activate or repress transcription (Strahl and Allis, 2000; Su and Denu, 2016); mitotically phosphorylated serine/threonine residues can regulate reader binding established at earlier stages of the cell cycle (Rossetto et al., 2012); or ubiquitinated lysine can impact the maintenance of DNA methylation (Vaughan et al., 2021). As the complex language of histone PTMs is being dissected, it has become clear that multivalent interactions with reader proteins can influence chromatin structure and DNA accessibility, thereby regulating gene transcription and other DNA-templated

events (Su and Denu, 2016; Taylor and Young, 2021; Young et al., 2010). In this manner, combinatorial PTMs can more effectively engage different chromatin-binding modules, promoting distinct outcomes versus either PTM alone.

The bulk of chromatin PTM research has employed histone peptides, even though histones exist *in vivo* in a heteromeric complex with DNA (i.e., the nucleosome). Recent work, however, is making it increasingly clear that studying histone PTM engagement in the nucleosome context provides a more accurate understanding of the histone code. Particularly, the highly charged histone tails interact directly with nucleosomal DNA, restricting access for PTM recognition by reader proteins (Ghoneim et al., 2021; Marunde et al., 2022a; Morrison et al., 2018). Studies with BPTF PHD suggest acetylation releases the H3 N-terminal tail from the nucleosome surface, such that H3K4me3 becomes more readily engaged by the PHD finger (Marunde et al., 2022a; Morrison et al., 2018).

Considerable research effort has focused on dissecting the direct (and multivalent) engagement of chromatin via histone PTM-reader protein interactions. However, less appreciated are any indirect effects of PTMs on histone tail accessibility/nucleosome dynamics (*e.g.,* via charge neutralization). In this report, we demonstrate enhanced nucleosome binding by a range of H3K4 readers when the histone tail is concomitantly acetylated (one or more of K9ac, K14ac, and K18ac). Furthermore, from *in vitro* enzymatic assays, we found that neighboring acetylation of the H3 tail is a prerequisite switch that enables the MLL1 complex (MLL1C) (Rao and Dou, 2015) to robustly methylate H3K4. Interestingly, mass spectrometric proteomic analyses of mammalian cells in a timed response to sodium butyrate (a broad-spectrum lysine deacetylase (KDAC) inhibitor) revealed a tight correlation of H3K4 methylation with *cis* acetylation. Our findings define a critical aspect of chromatin regulation: *i.e.,* histone crosstalk through acetylation-mediated tail accessibility. The findings also provide a molecular basis for the long-standing connection between H3K4 methylation and H3 acetylation in multiple eukaryotes (Garcia et al., 2007; Nightingale et al., 2007; Taverna et al., 2007), and resolve the directionality of these

correlations: *cis* hyperacetylation of the H3 tail precedes, and is largely a prerequisite for, H3K4 methylation. Thus, the establishment of sites of H3K4me3 and activation of transcription occur by a sequence of modifications of the same histone molecule.

RESULTS

PHD finger readers show narrowed selectivity for histone tail PTMs on mononucleosomes versus peptides

How histone readers engage nucleosomes is an extensively researched area of chromatin biology. Most investigators have used PTM-defined histone peptides to characterize reader binding, although these often display a refined preference to similarly modified nucleosomes (Marunde et al., 2022b, 2022a; Morgan et al., 2021; Morrison et al., 2018)**.** To further assess this potential, we used the dCypher® approach (Jain et al., 2020; Marunde et al., 2022b; Morgan et al., 2021; Weinberg et al., 2021) to measure the interactions of three PHD readers (from KDM7A, DIDO1, and MLL5: the queries) with PTM-defined peptides and nucleosomes (the potential targets). As expected (Jain et al., 2020), each GST-PHD fusion showed a preference for H3K4-methylated peptides and, particularly, to higher methyl states (*i.e.*, KDM7A bound me2/me3, DIDO1 bound me1/me2/me3, and MLL1 bound me1/me2/me3; **Figure 1A**). We further observed no impact of co-incident acetylation on H3K4me3 binding in the peptide context (compare H3K4me3 to H3K4me3K9acK14acK18ac [hereafter H3K4me3tri^{ac}]). However, on nucleosomes each GST-PHD showed reduced and restricted binding to H3K4me3 over the lower methyl states, and this interaction was dramatically enhanced (~10-15-fold) by co-incident acetylation (*i.e.*, H3K4me3tri^{ac}; **Figure 1B**). The notable impact of acetylation state on binding of these readers in the nucleosome context (also recently observed for the BPTF PHD domain (Marunde et al., 2022a; Morrison et al., 2018)) led us to consider additional implications of this interplay.

Histone tail lysine acetylation (Kac) can directly recruit residue-specific readers, *e.g.,* bromodomains (Musselman et al., 2012), but acetylation also neutralizes the positive charge on

lysine residues and relieves their interaction with negatively charged DNA (*i.e.*, altering the histone tail-DNA binding equilibrium) (Marunde et al., 2022a; Morrison et al., 2018). In the nucleosome context, this decreased histone-DNA binding supports the increased engagement of reader domains that have no direct affinity for the Kac. Conversely, isolated histone tail peptides are 'constitutively open' (no DNA to engage), and thus not subject to this mode of regulation. We surmised that the effect of charge neutralization to increase H3K4me3 accessibility could have application beyond reader domains, perhaps also applying to enzymes that target H3K4.

H3 N-terminal acetylation significantly enhances MLL1C methylation of nucleosomal H3K4

To investigate if acetylation might make the H3 N-terminus more accessible for modification, we performed enzymatic assays with the MLL1 core complex (MLL1C; responsible for H3K4me3) (Rao and Dou, 2015; Sha et al., 2020) and nucleosome substrates ± accompanying polyacetylation (H3K9acK14acK18ac; hereafter H3tri^{ac}) (see **Methods**). In an endpoint assay at constant enzyme and substrate concentrations (and [*methyl*-^{3}H]-SAM donor), we observed a significant increase in net methylation when the H3 tail was also acetylated (**Figure 2A**). As expected, methylation by MLL1C sequentially decreased towards H3K4 mono-, di-, and trimethylated nucleosomal substrates, being undetectable on H3K4me3 (which also confirmed MLL1C targeting of this specific residue). Despite this, methyl group incorporation to each H3K4 methyl state substrate was consistently enhanced by accompanying H3tri^{ac} (**Figure 2A**). Of note, we also tested the viability of synthetic methyllysine analogs (MLAs) (Simon and Shokat, 2012) ± H3tri^{ac} as MLL1C substrates and observed no activity, indicating the unsuitability of MLAs for such studies (**Figure S2D**).

We also measured the steady-state kinetics of MLL1C methylation of nucleosomes with each H3K4 methyl state ± H3tri^{ac}, and again observed that acetylation increased methyltransferase activity (**Figure 2B**). Using an extra sum-of-squares F-test, methylation data for the H3tri^{ac} nucleosomes were indicative of positive cooperativity because of better fit (p =

0.0216) to the Hill equation (Weiss, 1997) (**Figure 2B** v. **Figure S2C**; **Table 1** v. **Table S1**). Because of the low level of enzymatic activity towards the unacetylated nucleosomes we could not make a statistically significant comparison between the Hill and Michaelis-Menten fits. There have been limited studies of MLL1C activity on nucleosomes (Park et al., 2019; Patel et al., 2011; Xue et al., 2019), so an overlooked potential allostery is understandable given the many possible interactions between this enzyme complex and substrate (Lee et al., 2021; Park et al., 2019).

Interestingly, although overall k_{cat} was ~17-fold greater for the H3tri^{ac} nucleosomes, the $K_{0.5}$ values (substrate concentration at half-maximal velocity/half-saturation for an allosterically regulated enzyme) were indistinguishable (**Table 1**). Therefore, although MLL1C catalytic efficiency toward H3tri^{ac} nucleosomes was enhanced by an increase in k_{cat}, this catalytic efficiency was not driven by $K_{0.5}$, which suggested no increase in relative binding affinity. To further examine this, we used dCypher to examine potential binding between MLL1C query and a selection of nucleosome targets: unmodified, H3NΔ32 (lacking the first 32 residues of H3), Tailless (trypsin-digested nucleosomes to remove N- and C-terminal histone tails), and H3tri^{ac}. At 50 mM NaCl, we observed no compelling difference in MLL1C binding between any of these nucleosomes (**Figure 2C**). This finding agreed with structural studies where binding between MLL1C and the nucleosome occurs primarily through interactions with nucleosomal DNA and, to a lesser degree, the H4 N-terminal tail (Lee et al., 2021; Park et al., 2019). Thus, the increased H3K4 methylation observed when the H3 N-terminal tail was acetylated is not due to enhanced MLL1C – nucleosome binding. Instead, H3 acetylation likely released the histone tail from the nucleosome, thereby increasing the apparent H3K4 concentration for MLL1C and enhancing methylation (**Figure 2D**).

Cellular level of H3K4 methylation is coupled to H3 N-terminal tail hyperacetylation

The above data suggested a molecular model for how the H3 N-terminal tail, via *cis* acetylation, becomes available for H3K4 reader binding or enzymatic modification *in vitro*. To determine if

159 such acetylation could function as an accessibility switch *in vivo*, we developed a novel targeted
160 middle-down mass spectrometry method to provide a single molecule quantitative measure of
161 histone tail modification. We applied this method to acid-extracted histones from asynchronous
162 MCF-7 breast cancer cells to measure the relationship between H3K4 methylation and tail
163 acetylation on the same H3 proteoforms (Holt et al., 2021; Smith and Kelleher, 2013). As expected
164 (Garcia et al., 2007; Peach et al., 2012; Young et al., 2009), the absolute amounts of H3K4me3
165 and higher Kac states (3ac, 4ac, and 5ac) across adjacent lysine residues were extremely low
166 (**Figure S3A**). Nonetheless, H3K4me3 (<1% of total H3) was strictly associated with molecules
167 that contained multiple acetylations (also <1% of total H3; **Figure 3A**). Given this relationship, we
168 next addressed the hypothesis that increased lysine acetylation may release the H3 tail for more
169 effective H3K4 methylation (*i.e*., acetylation precedes methylation). We treated MCF-7 cells with
170 the KDAC inhibitor sodium butyrate and collected samples at multiple timepoints to measure the
171 levels of H3K4 methylation with *cis* acetylation. H3 poly-acetylation rapidly increased upon
172 butyrate treatment (**Figure S3B** and **Table S2**), as expected (Holt et al., 2019; Young et al., 2009).
173 While H3K4me3 levels most dramatically increased in tandem with the 5ac H3 state (**Figure 3B**),
174 we observed an associated increase in all H3K4 methyl states, relative to the unmodified state,
175 as the H3 tail was increasingly acetylated (**Figures 3C** and **3D; Table S2**). An example of tandem
176 mass spectra at each acetyl degree, showing the $C4^{+1}$ ion series from which K4 stoichiometry is
177 measured, are shown in **Figure 3D**. These findings support a direct link whereby acetylation
178 releases nucleosome-bound H3 tails to available H3K4 methyltransferases for subsequent
179 methylation (see model in **Figure 2D**). Such a chromatin-switch may also help cells to translate
180 short-term acetylation signals at gene promoters to longer-term heritable marks of epigenetic
181 memory (Greer et al., 2014; Hörmanseder et al., 2017; Muramoto et al., 2010; Ng et al., 2003).
182
183 **DISCUSSION**

While previous investigations identified a link between H3K4 methylation and H3 acetylation in diverse species (Garcia et al., 2007; Nightingale et al., 2007; Strahl et al., 1999; Taverna et al., 2007; Young et al., 2009) the molecular basis for this link was unknown, and we posit the H3 acetyl 'chromatin switch' defined herein is conserved across eukaryotes. Our new understanding of the dynamic structure of nucleosome histone tails, alternating between collapsed (*i.e.*, nucleosome-bound) and accessible forms (Marunde et al., 2022a; Morrison et al., 2018), has made more plausible the notion that tail availability could be driven by combinatorial *cis* acetylation to directly promote H3K4 methylation. In this study, we showed that hyperacetylation of the H3 N-terminal tail promoted rapid accumulation of H3K4 methylation in *cis*, most likely by increasing availability of the substrate residue to the MLL1C active site. This finding was supported by our *in vitro* enzymatic and *in vivo* mass spectrometric analyses. Methylation assays with MLL1C revealed significantly enhanced enzyme activity towards nucleosome substrates with co-incident acetylated (H3tri^{ac}) over unmodified H3 (**Figure 2A-B; Table 1**). dCypher assays demonstrated that the acetylation-mediated increase in H3K4 methylation does not involve stabilized interactions between MLL1C and the nucleosome (**Figure 2C**). In agreement with these *in vitro* findings, middle-down mass spectrometry showed that H3 hyperacetylation and H3K4 methylation co-occurred on the same histone tails in actively cycling cells; furthermore, upon butyrate treatment H3K4 methylation increased for the most highly acetylated proteoforms (**Figures 3** & **S3**). The *in vivo* relationship required higher degrees of acetylation (preferring at least four acetyl groups per molecule: *e.g.*, H3K9acK14acK18acK23acK27ac) for most effective conversion to the H3K4me3 state. This is likely a function of yet to be explained *in vivo* acetylation hierarchies by KATs that are outside the scope of this study but will be important to resolve. Together with binding studies that identify the positive impact of *cis* H3 tail hyperacetylation on H3K4 reader engagement (**Figures 1** & **S1**) (Marunde et al., 2022a; Morrison et al., 2018), our findings suggest a molecular switch that governs when and where the histone H3 N-terminus is

209 available for H3K4-related transactions. Such a switch could be used to establish and heritably
210 maintain the location and function of transcriptional promoters across the genome.

211 A continued observation from this study is that the binding preference of readers (in this
212 case PHD-fingers that engage histone H3K4) are narrowed on nucleosomes relative to histone
213 peptides (**Figure 1** & **S1**) (Marunde et al., 2022a; Morgan et al., 2021). This difference in binding
214 further highlights the importance of using nucleosomes as physiologically relevant substrates for
215 *in vitro* interaction assays. We also add to the literature confirming importance of the physiological
216 substrate for enzymatic studies (Strelow et al., 2016; Stützer et al., 2016). In this regard our
217 steady-state kinetic methylation assays with MLL1C revealed an intriguing (and previously
218 undescribed) positive cooperativity with its preferred nucleosome substrates (**Figure 2B** versus
219 **S2C**). It is important to consider the suggestion that allosteric factors could regulate interactions
220 between MLL1C and the nucleosome, especially since previous kinetic analyses of this
221 [enzyme:substrate] pair did not address such behavior (Park et al., 2019; Xue et al., 2019).
222 However, positive cooperativity was not evident at the level of MLL1C - nucleosome binding,
223 which was independent of substrate identity (*i.e.*, ± H3tri^{ac}) at ionic conditions similar to the
224 catalytic assay (**Figure 2C**). Still to be determined are the signals that drive and regulate this
225 cooperativity and its function in MLL1-catalyzed methylation, especially in a higher-order
226 chromatin context.

227 Taken together, our study highlights a previously unrecognized regulatory mechanism for
228 how writers might engage the histone H3 tail (specifically at H3K4) *in vivo*. Although this work
229 focused on H3K4, it will be important to ascertain the consequence of acetylation (or acylation)-
230 mediated changes in accessibility and the function of modifiers and readers of the other lysines
231 on H3 as well as the other core histones (H2A, H2B, and H4). Underscoring the need for such
232 studies, we note recent *in vitro* analyses employing unmodified nucleosomes sequentially
233 targeted by purified KATs and KMTs suggest that the acetylation landscape can impact multiple
234 methyltransferases (Trush et al., 2022). The field will require a more detailed analysis of the *in*

235 *vivo* contributions of various KATs/KDACs in regulating histone tail accessibility (in *cis* and *trans*)
236 for other chromatin-modifying enzymes to further uncover the molecular details of the histone
237 code.

238 Finally, we note that many studies have identified H3K4 methylation and H3 acetylation
239 as active marks because of their co-occupancy on the promoters and gene bodies of transcribed
240 genes (Santos-Rosa et al., 2002; Strahl et al., 1999; Wozniak and Strahl, 2014). Our findings
241 agree with these observations, but importantly, uncover a previously unrecognized mechanism of
242 H3 cross-talk that impinges on fundamental functions of H3 acetylation and K4 methylation in
243 gene regulation. Given its importance, we predict this regulatory mechanism may be a target for
244 dysregulation in human disease.

ACKNOWLEDGEMENTS

KJ is supported by a Postdoctoral Training Fellowship from the National Institutes of Health (NIH; T32CA217824) to the UNC Lineberger Cancer Center and a Postdoctoral Fellowship from the American Cancer Society (PF-20-149-01-DMC). This work was also supported by NIH grants to NLY (R01GM139295, P01AG066606, and R01CA193235), MSC (R01CA140522), *EpiCypher* (R44GM117683, R44CA214076 and R44GM116584), and to BDS (R35GM126900). We thank colleagues for the generous supply of materials (see **Methods**) and members of the Cosgrove, Young, *EpiCypher* and Strahl labs for helpful discussions and suggestions.

AUTHOR CONTRIBUTIONS

KJ, MRM, JMB, NLY, MCK, and BDS conceptualized and designed the study. ZBG, SAH, MAC, and MJM assembled and validated PTM-defined dNucs and versaNucs. KK synthesized histone peptides used in versaNuc construction. MM, JB, SLG, KLR, IKP, NWH, AV, and ENW performed dCypher assays and analyzed data with input from KJ, MCK, and BDS. KEWN and MSC purified MLL1C for enzymatic analyses. KJ and SWC purified his-tagged MLL1C for binding assays. Methylation assays were performed and analyzed by KJ, SWC, and GCF. MCF7 cells were cultured by KJ, and mass spectrometry was performed and analyzed by FJ, BCT, and NLY. KJ and BDS wrote the first draft of the manuscript and all authors contributed to subsequent editing.

DECLARATIONS OF INTEREST

MSC owns stock/serves on the Consultant Advisory Board for Kathera Bioscience Inc. and holds US patents (8,133,690; 8,715,678; and 10,392,423) for compounds/methods for inhibiting SET1/MLL family complexes. *EpiCypher* is a commercial developer and supplier of reagents (e.g., PTM-defined semi-synthetic nucleosomes; dNucs™ and versaNucs®) and platforms (*e.g.,* dCypher®) used in this study. MCK and BDS are board members of *EpiCypher*.

FIGURE LEGENDS

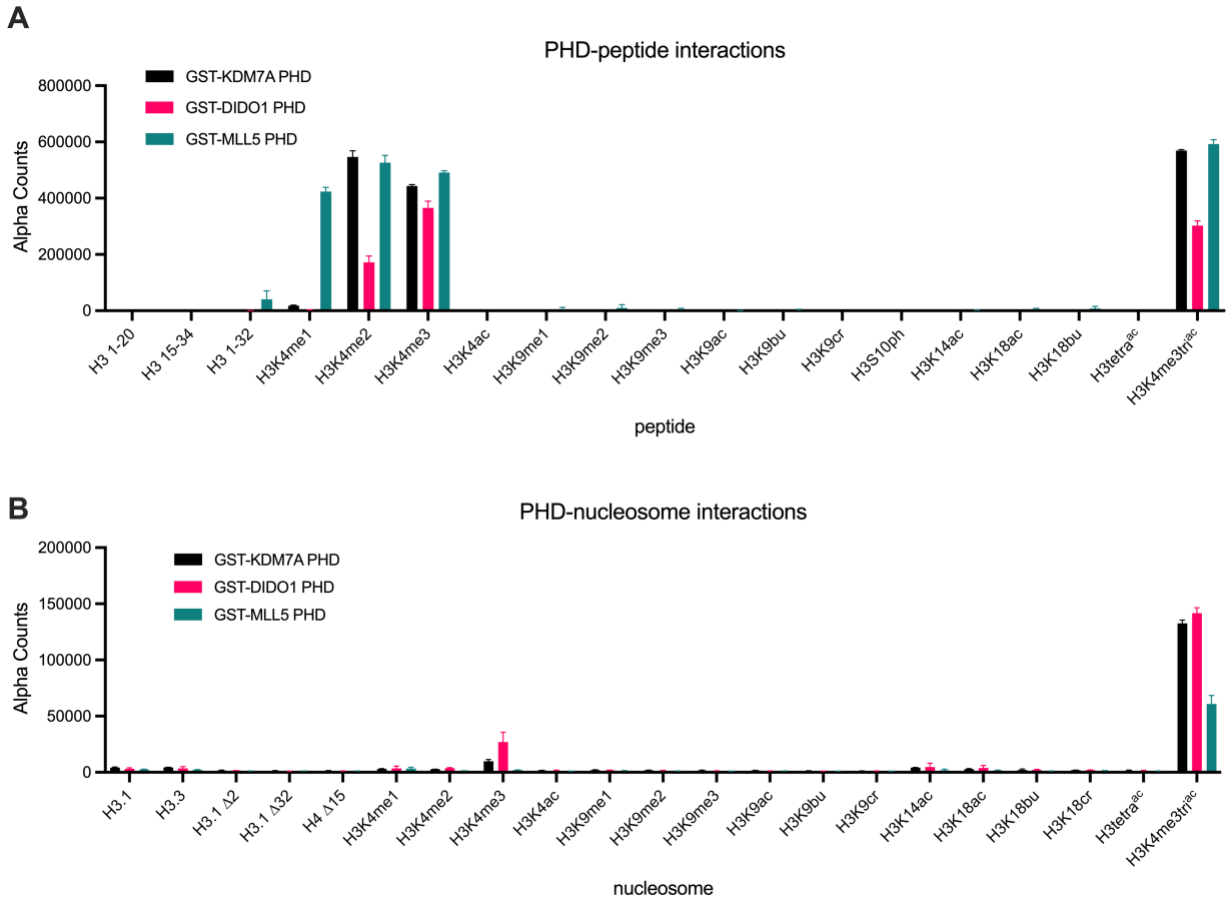

Figure 1. PHD finger reader domains show restricted binding on PTM-defined peptides vs. nucleosomes. *dCypher* assay alpha counts for interaction of GST-PHD queries (9.5 nM KDM7A (Uniprot #Q6ZMT4; residues 1-100); 2.4 nM DIDO1 (Uniprot #Q9BTC0; residues 250-340); 18 nM MLL5 (Uniprot #Q8IZD2; residues 100-180)) with PTM-defined peptides (**A**) *vs.* nucleosomes (**B**) (the potential targets). All error bars represent the range of two replicates. Key: H3.1 Δ2, H3.1 Δ32 and H4 Δ15 are nucleosomes assembled with histones lacking the indicated N-terminal residues of H3.1 or H4. All data was plotted using GraphPad Prism 9.0.

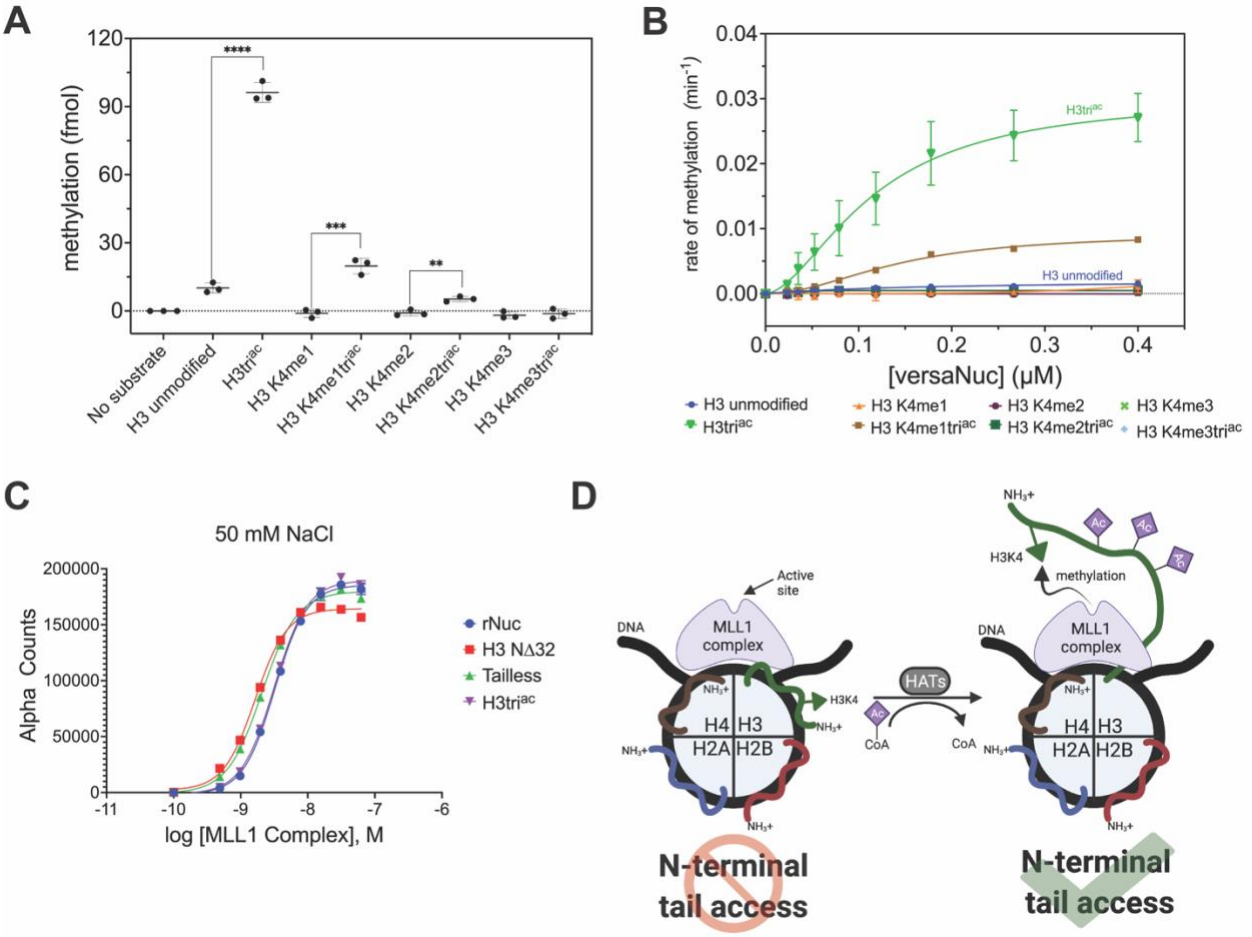

Figure 2. In the nucleosome context MLL1C methylation activity on H3K4 is significantly enhanced by co-incident H3tri^{ac}. **A)** Endpoint methylation assays of H3K4me0 (unmodified)-me1-me2-me3 nucleosomes and their cognate H3K9ac14ac18ac (H3tri^{ac}) partners (all 100 nM) with MLL1C (4nM). Reactions performed in triplicate with error bars as S.E.M. *p*-values were determined using a two-tailed t test: **** = <0.0001, *** = 0.0008, ** = 0.0038. **B)** MLL1 complex (MLL1C; 4 nM) methylation activity on H3K4me0-me1-me2-me3 nucleosomes and their cognate H3tri^{ac} partners (all substrates: 1.5-fold serial dilution, 0-0.4 μM). Reactions performed in triplicate with error bars as S.E.M. **C)** dCypher binding curves of 6HIS-tagged MLL1C (concentration as noted) with PTM-defined nucleosomes (20 nM). Error bars represent the range of two replicates. **D)** Graphical model for how H3 N-terminal tail acetylation may regulate H3K4 methylation by

293 MLL1C. Nucleosomal DNA is represented in black; each histone is as labeled, with the core
294 histone N-terminal tails colored to distinguish. MLL1C is in purple.
295

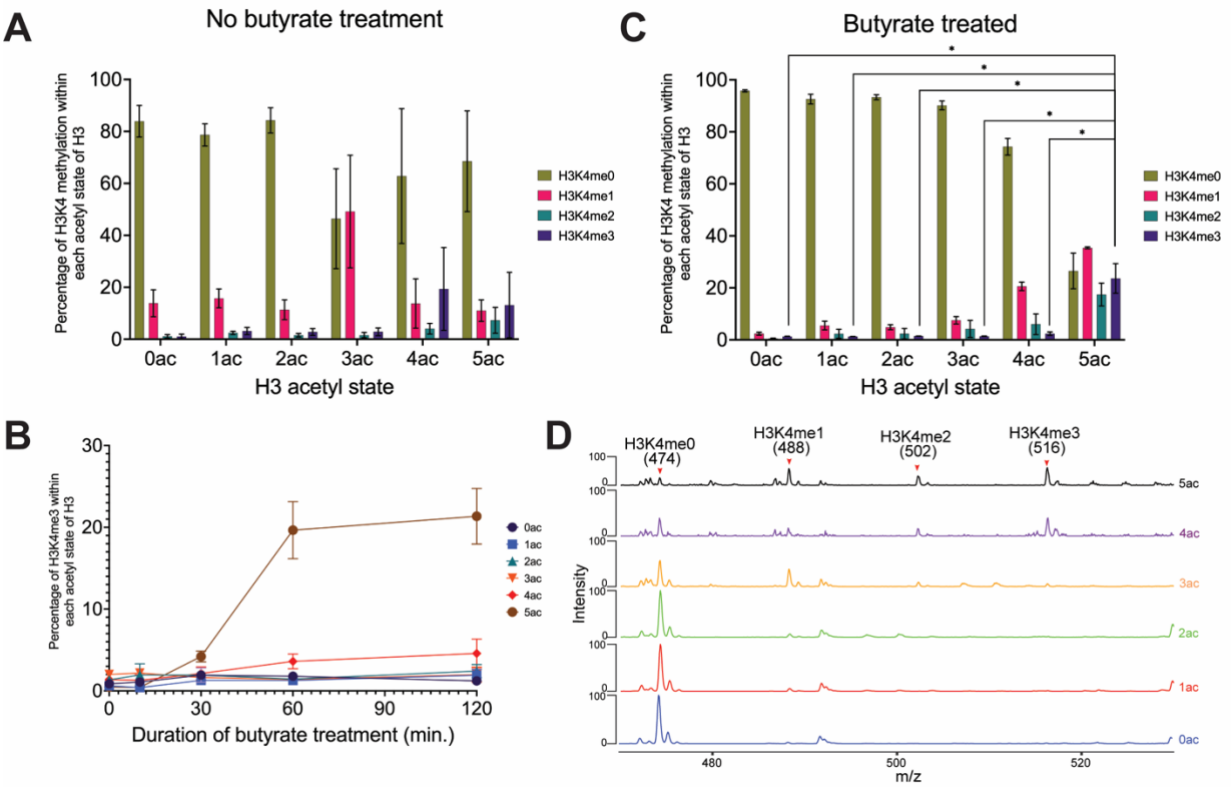

296

297 **Figure 3. Middle-down MS analysis reveals a hierarchical dependence between H3K4**
298 **methylation and *cis* H3 acetylation in MCF-7 cells. A)** Occupancy of H3K4 methyl states (me0-
299 1-2-3) within each H3 acetyl state (0ac to 5ac) in asynchronous MCF-7 cells. **B)** Time course of
300 H3K4me3 accumulation with respect to each H3 acetyl state after butyrate treatment. **C)**
301 Occupancy of H3K4 methyl states within each H3 acetyl state after butyrate treatment (60 mins).
302 Asterisks represent *p*-values < 0.05. **D)** Representative tandem mass spectra of the targeted $C4^{+1}$
303 fragment ion series (474 *m/z* unmodified; 488 *m/z* me1; 502 *m/z* me1; 516 *m/z* me3). Each
304 spectrum is an average of MS2 spectra of the indicated H3 acetyl states after 60 minutes of
305 butyrate treatment. This figure directly shows that K4 occupancy stoichiometry correlated with H3
306 acetylation state and that the targeted MS method provides excellent signal-to-noise for confident

307 quantitation. See **Methods** for further information on data acquisition and analysis. All data were

308 collected in biological triplicate with error bars representing S.E.M.

TABLES

TABLE 1: Steady-state Hill kinetic parameters

Substrate	$K_{0.5}$ (μM)	k_{cat} (min^{-1})	h (Hill coefficient)	R^2
H3 unmodified	0.13 ± 0.06	0.0018 ± 0.0004	1.213 ± 0.3430	0.8810
H3 K9ac/14ac/18ac	0.12 ± 0.02	0.0304 ± 0.0036	1.741 ± 0.3528	0.9228
H3K4me1	n.d.[a]	n.d. [a]	n.d. [a]	0.3186
H3K4me1 K9ac/14ac/18ac	0.14 ± 0.008	0.0092 ± 0.0004	2.032 ± 0.1333	0.9920
H3K4me2	n.d. [a]	n.d. [a]	n.d. [a]	-0.1746
H3K4me2 K9ac/14ac/18ac	0.042 ± 0.005	0.0005 ± 0.00004	5.349 ± 2.682	0.8155
H3K4me3	n.d. [a]	n.d. [a]	n.d. [a]	n.d. [a]
H3K4me3 K9ac/14ac/18ac	n.d. [a]	n.d. [a]	n.d. [a]	n.d. [a]

[a] = methylation signal was indistinguishable from background: kinetic parameters could not be determined.

METHODS

Expression and purification of GST-tagged PHD reader proteins

Recombinant expression constructs for GST-tagged PHD domains from KDM7A (Uniprot #Q6ZMT4; residues 1-100), DIDO1 (Uniprot #Q9BTC0; residues 250-340), and MLL5 (Uniprot #Q8IZD2; residues 100-180) were synthesized by BioMatik Corporation in a pGEX-4T-1 vector and provided by Dr. Mark T. Bedford (UT MD Anderson Cancer Center). These proteins were expressed and purified as described (Jain et al., 2020).

Expression, purification, and assembly of the MLL1 core complex (MLL1C)

Methods for the expression, purification, and assembly of MLL1 core complex (MLL1C) were adapted from published protocols (Usher et al., 2021). A polycistronic recombinant expression construct containing the MLL1 SET domain (Uniprot Q03164; residues 3745-3969), WDR5 (Uniprot P61964; residues 2-334), RbBP5 (Uniprot Q15291; residues 1-538) and Ash2L (Uniprot Q9UBL3-3; residues 1-534) (MWRA construct) in pST44 vector was a kind gift from Dr. Song Tan (Tan et al., 2005). WDR5 was cloned with an N-terminal hexahistidine (6HIS) tag and TEV protease site to enable purification via immobilized metal affinity chromatography (IMAC), and enzymatic cleavage for tag removal. Rosetta pLysS *E. coli* cells were transformed with the plasmid and grown on LB plates with 50 μg/mL carbenicillin. Single colonies were used to inoculate 50 mL starter cultures of Terrific Broth (TB) containing 50 μg/mL carbenicillin and grown at 37°C for 16 hours. This culture was transferred to 1L of TB + carbenicillin and grown to OD_{600} ~0.6 (37°C, 200 RPM, ~ 4 hours). Recombinant protein expression was induced with 1 mM Isopropyl β-D-1-thiogalactopyranoside (*Sigma*; 16°C, 200 RPM, 20 hours). Cells were harvested by centrifugation (5000 RPM, 4°C) and flash frozen in liquid nitrogen.

Frozen cell pellets were resuspended in 50 mL of lysis buffer (50 mM Tris-HCl pH 7.5, 300 mM NaCl, 30 mM imidazole, 3 mM dithiothreitol, and 1 μM $ZnCl_2$) containing 0.5 mg/mL lysozyme

(*Sigma*), 250 U Pierce Universal Nuclease (*ThermoFisher*), and an EDTA-free protease inhibitor cocktail (*Roche*) and rotated at 4°C for 1 hour. The resultant mixture was then sonicated [five cycles of 30 sec on/30 sec off at 50% output] and centrifuged at 4°C, 15,000 RPM for 35 min. The clarified lysate was flowed over a 5 mL HisTrap nickel column (*Cytiva*) using an AKTA Pure FPLC (*Cytiva*) at 0.5 mL/min; all FPLC steps were conducted at 4°C. Unbound molecules were removed with 20 column volumes of wash buffer (WB: 50 mM Tris-HCl, pH 7.5, 300 mM NaCl, 30 mM imidazole, 3 mM DTT, and 1 µM $ZnCl_2$ at 2 mL/min). The 6HIS-tagged MWRA was eluted in a 15-column volume linear gradient from WB to Elution Buffer (WB + 500 mM imidazole) at 2 mL/min. Fractions containing 6HIS-tagged MWRA were identified by SDS-PAGE, pooled, and supplemented with 6HIS-tagged TEV protease (purified as described: Nautiyal and Kuroda, 2018) at a 1:100 enzyme to substrate molar ratio to cleave the 6HIS-tag on WDR5. This mixture was dialyzed against three changes of WB (each 2L for at least four hours at 4°C) and 6HIS-TEV removed from cleaved MWRA via IMAC (Usher et al., 2021). MWRA flow-through protein solution was concentrated to ~15 mL using a 30 kDa MWCO centrifugal filter (*EMD Millipore*), ensuring not to concentrate to where solution became yellow/cloudy and viscous. MWRA complex was resolved over a HiLoad 16/60 Superdex 200 pg gel filtration (GF) column (*Cytiva*) pre-equilibrated in 20 mM Tris-HCl, pH 7.5, 300 mM NaCl, 1 mM TCEP, and 1 µM $ZnCl_2$. Fractions containing stoichiometric MWRA sub-complex were identified by SDS-PAGE, pooled, and concentrated to ~15 mL.

HisDPY30 was expressed, purified, and cleaved to remove the 6HIS-tag as described (Patel et al., 2009; Usher et al., 2021). A two-fold molar excess of DPY30 was added to the MWRA sub-complex and incubated on ice for 1 hour. Following incubation, MLL1C was isolated by gel filtration as described for the MWRA complex, with fractions containing the stoichiometric complex identified by SDS-PAGE, pooled, concentrated to ~10 µM, and flash frozen. For dCypher experiments with MLL1C, the 6HIS-tag was retained on DPY30.

366 *PTM-defined nucleosomes*

367 All nucleosomes were from the dNuc™ or versaNuc® portfolios (*EpiCypher*). PTMs were
368 confirmed by mass-spectrometry and immunoblotting (if an antibody was available) (Goswami et
369 al., 2021; Marunde et al., 2022b; Weinberg et al., 2019).

370

371 *dCypher assays*

372 *dCypher* binding assays with PTM-defined nucleosomes were performed under standard
373 conditions that titrate query (*e.g.,* epitope-tagged reader domain(s)) to a fixed concentration of
374 target (*e.g.*, biotinylated PTM-defined nucleosome) with the appropriate Alpha Donor and
375 Acceptor beads (*Perkin Elmer*) (Jain et al., 2020; Marunde et al., 2022b; Weinberg et al., 2019).
376 Binding curves [query:target] were generated using a non-linear 4PL curve fit in Prism 9.0
377 (*GraphPad*). For each query, the relative EC_{50} (EC_{50}^{rel}) and hillslope values were derived from the
378 best binding target. EC_{50}^{rel} is the half maximal signal for the specified target. Where necessary,
379 we excluded query concentration values determined to be beyond a query's hook point (signal
380 inhibition due to query exceeding bead saturation). The EC_{80}^{rel} was selected as the optimal
381 probing concentration for discovery screens because of the robust signal-to-background and to
382 provide the best opportunity to bind targets without saturating the primary target signal. To
383 compute EC_{80}^{rel} values, we used the formula $EC_F^{rel} = (F/ (100 – F)^{1/H} \times EC_{50}^{rel}$; F = 80 and H =
384 hillslope.

385 Briefly, 5 µL of GST-tagged reader domain was incubated with 5 µL of 10 nM biotinylated
386 nucleosomes (*e.g., EpiCypher* #16-9001) for 30 minutes at room temperature in 20 mM HEPES
387 pH 7.5, 250 mM NaCl, 0.01% BSA, 0.01% NP-40, 1 mM DTT in a 384-well plate. A mix of 10 uL
388 of 2.5 µg/mL glutathione acceptor beads (*PerkinElmer*, AL109M) and 5 µg/mL streptavidin donor
389 beads (*PerkinElmer*, 6760002) was prepared in 20 mM HEPES pH 7.5, 250 mM NaCl, 0.01%
390 BSA, 0.01% NP-40 and added to each well. The plate was incubated at room temperature in
391 subdued lighting for 60 minutes, and AlphaLISA signal was measured on a PerkinElmer 2104

392 EnVision (680 nm laser excitation, 570 nm emission filter ± 50 nm bandwidth). Each binding
393 interaction was performed in duplicate in a 20 µL mix in 384 well plates.
394 MLL1C binding assays (**Figure 2C**) were performed as described above except using
395 Nickel-chelate acceptor beads (10 µg/mL; *Perkin Elmer* AL108M), streptavidin donor beads (20
396 µg/mL; *Perkin Elmer*) and modified assay buffer (20 mM Tris pH 7.5 + 50 mM NaCl, 0.01% BSA,
397 0.01% NP-40 and 1 mM DTT); [NaCl] was optimized via a titration assay and 50 mM chosen for
398 subsequent analyses.
399
400 In vitro *methylation assays*
401 Methylation assays (Shinsky et al., 2015) were performed at 15°C for three hours using purified
402 MLL1C enzyme and nucleosome substrate in a reaction volume of 20 µL [in 50 mM HEPES, pH
403 8.0, 1 mM DTT, 1 µM $ZnCl_2$; 10 µM of 9:1 *S*-adenosyl-L-methionine (SAM) *p*-toluenesulfonate
404 salt (*Sigma*) to *S*-adenosyl-L-[*methyl*-^{3}H]-methionine ([*methyl*-^{3}H]-SAM) (*PerkinElmer*)].
405 Concentrations of MLL1C and NaCl were optimized from 2D-titration methylation assays at [0, 4
406 and 40 nM MLL1C] and [0, 50 and 300 mM NaCl] with 2 µg of chicken oligo-nucleosome substrate
407 (Morris et al., 2007). It is notable that, across a range of concentrations, MLL1C stability
408 decreases as temperature increases and methyltransferase activity has been reported to be
409 enhanced in sub-physiological NaCl concentrations (Namitz et al., 2019; Shinsky et al., 2015).
410 For endpoint methylation assays, 4 nM MLL1C and 100 nM nucleosome substrates were tested
411 as above. For steady-state kinetics, 4 nM MLL1C was incubated with a nucleosome substrate
412 titration (0, 23.4, 35.1, 52.7, 79, 119, 178, 267 and 400 nM) and reactions quenched with 5 µL of
413 5X SDS loading dye. For steady-state kinetic assays, 0.5 µg bovine serum albumin was added to
414 each reaction after quenching to act as a loading guide. To analyze methylation, quenched
415 reactions were resolved by 15% Tris-Glycine SDS-PAGE. Gels were stained with Coomassie dye
416 and bands containing mononucleosomes were excised (with serum albumin as a supporting lane
417 marker) and incubated in a solution of 50% Solvable (*PerkinElmer*) and 50% water at 50°C for

three hours. Mixture and gel slices were then combined with 10 mL of Hionic-Fluor scintillation fluid (*PerkinElmer*), dark-adapted overnight, and radioactivity measured on a Liquid Scintillation Counter (*Beckman Coulter*).

Middle-down mass spectrometry of MCF-7 cells ± KDAC inhibition

MCF-7 breast cancer cells (ATCC HTB-22) were grown in MEM (*Gibco*) supplemented with 10% fetal bovine serum (*VWR*), 100 I.U. penicillin, 100 µg/mL streptomycin (*Corning*), 0.01 mg/mL human recombinant insulin (*Gibco*), and 5 µg/mL plasmocin (*Invivogen*) at 37°C and 5% CO_2.

For mass spectrometric (MS) analysis ± KDAC inhibition, cells were cultured in 150 mm dishes to ~80% confluence and treated with 5 mM sodium butyrate (or equivalent volume of water) in triplicate for 0, 10, 20, 30, 60, 120 mins. Cells were washed with cold PBS (11.9 mM phosphates, 137 mM NaCl, 2.7 mM KCl) to remove residual sodium butyrate, harvested by scraping, and flash frozen in liquid nitrogen. Histones were acid extracted after nuclei isolation as described (Holt et al., 2021). Isolated histones were resuspended in 85 µL 5% acetonitrile, 0.2% trifluoroacetic acid (TFA) and resolved by offline high-performance liquid chromatography (HPLC) as described (Holt et al., 2021). Reverse Phase HPLC fractionation was performed with a U3000 HPLC system (*ThermoFisher*) with a 150 × 2.1–mm Vydac 218TP 3 µm C18 column (*HiChrom* # 218TP3215), at a flowrate of 0.2 mL/min using a linear gradient from 25% B to 60% B in 60 min. The composition of buffers used were A: 5% acetonitrile and 0.2% TFA and B: 95% acetonitrile and 0.188% TFA. After chromatographic separation and fraction collection, histone H3.1 was selected, diluted in 100 mM ammonium acetate (pH = 4) and digested with Glu-C protease (*Roche*) at 10:1 protein:enzyme for 1 h at room temperature prior to mass spectrometric analysis.

The digested samples were diluted to 2 µg/µL. Online HPLC was performed on a U3000 RSLC nano Pro-flow system using a C3 column (Zorbax 300SB-C3, 5 µm; *Agilent*). Samples were maintained at 4 °C and 1 µL injected for each analysis using a microliter pickup. A linear 70-minute gradient of 4-15% B was used (Buffer A: 2% acetonitrile, 0.1% formic acid and Buffer B:

98% acetonitrile and 0.1% formic acid) with a flow rate of 0.2 µL/min. The column eluant was introduced into an Orbitrap Fusion Lumos mass spectrometer (*ThermoFisher*) by nano-electrospray ionization. A static spray voltage of 1900 V and an ion transfer tube temperature of 320 °C were set for the source.

A Fusion Lumos mass spectrometer was used to generate MS the data. The 9th charge state of histone H3 was targeted for analysis. MS1 analysis was acquired in the orbitrap with a normal mass range and a 60k resolution setting in positive ion mode. An Automatic Gain Control (AGC) target of 5.0E5 with a 200 ms maximum injection time, three microscans, and a scan range of 585-640 *m/z* were used to identify desired ions for fragmentation. MS2 acquisition was performed in both orbitrap and ion trap mode. Both modes used electron transfer dissociation (ETD), a reaction time of 18 ms, and an injection time of 200 ms. A normal scan range was used for the orbitrap mode with a resolution setting of 30k and an AGC target of 5.0E5, with two micro scans. A narrow scan range of 470-530 *m/z*, targeting ions indicative of K4 modification states, was used for the ion trap mode MS2 with an ACG target of 3.0E4, quadrupole isolation, maximum injection time of 100 ms, and eight microscans.

These MS methods were used with two technical replicates per biological replicate (n=3). An MS ion trap mode with a targeted mass list was used to increase sensitivity to identify known low abundance K4me3-containing proteoforms. The ion trap MS2 spectra were averaged for each H3 acetyl state based on known retention times, and the intensities of ions indicative of the K4 methylation states were manually recorded. Retention times for each acetyl state were approximated as 0ac 35-40 min, 1ac 45-55 min, 2ac 55-60 min, 3ac 62-68 min, 4ac 69-73 min, and 5ac 74-78 min. Precursor mass was used as an additional confirmation and filter of correct acetyl state. For scans yielding low signal and high noise (*i.e.,* 5ac at 0 min butyrate treatment), data were manually curated before averaging. Within acetyl states, the relative proportion of fragment ions for unmodified, mono-, di-, and trimethylation of the H3K4 ion at respective *m/z* of 474, 488, 502, and 516 were recorded per MS run. Values were averaged across replicates of

the same conditions and normalized to one hundred percent. A two-tailed t-test was used for significance. Raw MS data is available at (ftp://massive.ucsd.edu/MSV000089089/).

The MS method used here is highly targeted to most effectively address the mechanistic or single molecule link between H3 acetylation degree and H3K4 occupancy. The strategy used prioritizes optimization of efficient selection of acetyl degree and of the signal-to-noise for the $C4^{+1}$ ion series. This is to the exclusion of other information that can typically be derived from untargeted approaches. For example, because trapping mass spectrometers are limited in the number of ions, we dispose of unnecessary ions to gas phase enrich the C4 ions series. This method provides a direct measure of stoichiometry of K4un, K4me1, K4me2, and K4me3 within an acetyl state.

SUPPLEMENTAL INFORMATION

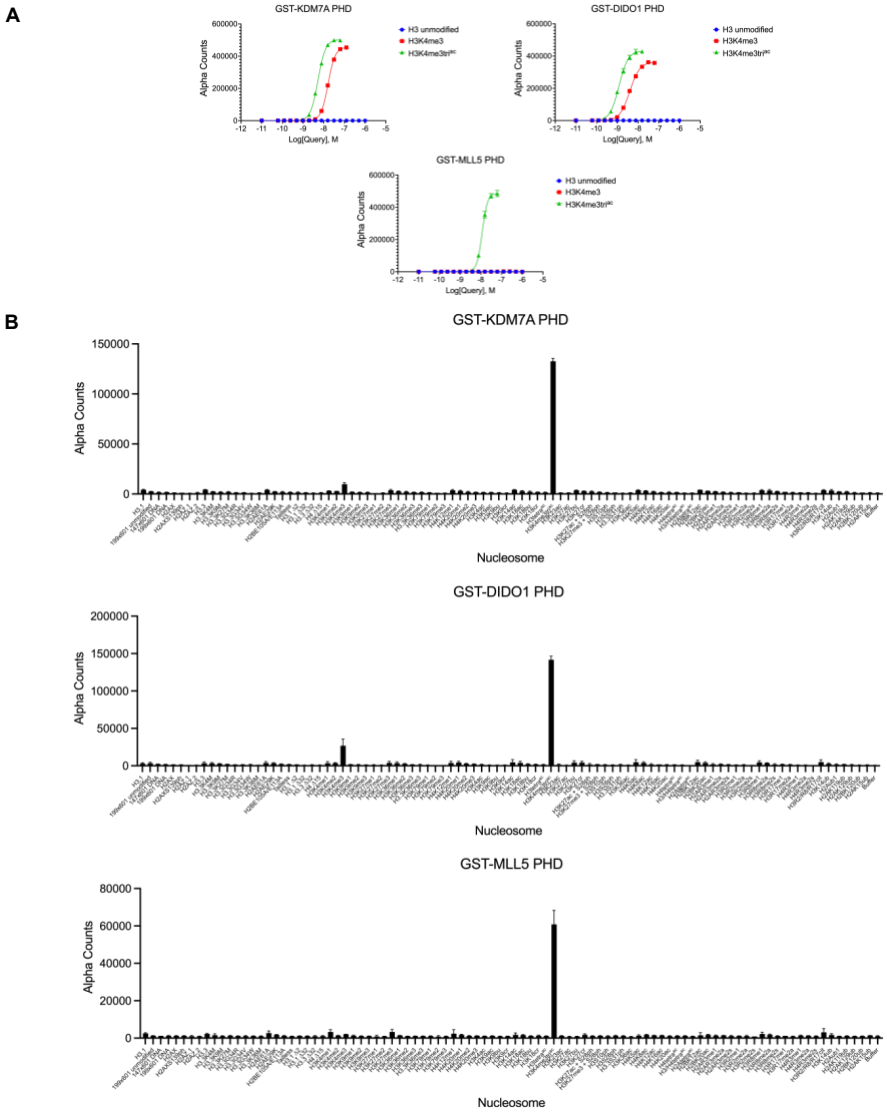

Figure S1. dCypher assay with three PHD finger-containing proteins. A) Binding curves to determine optimal concentration for screening reader queries (GST-KDM7A (PHD), GST-DIDO1 (PHD), and GST-MLL5 (PHD)) to indicated PTM-defined nucleosome targets. **B)** Library binding screen with indicated PHD queries and PTM-defined nucleosome targets. Error bars represent

the range of two replicates. Key: H3.1N Δ2, H3.1N Δ32 and H4N Δ15 are nucleosomes assembled with histones lacking the indicated N-terminal residues of H3.1 or H4.

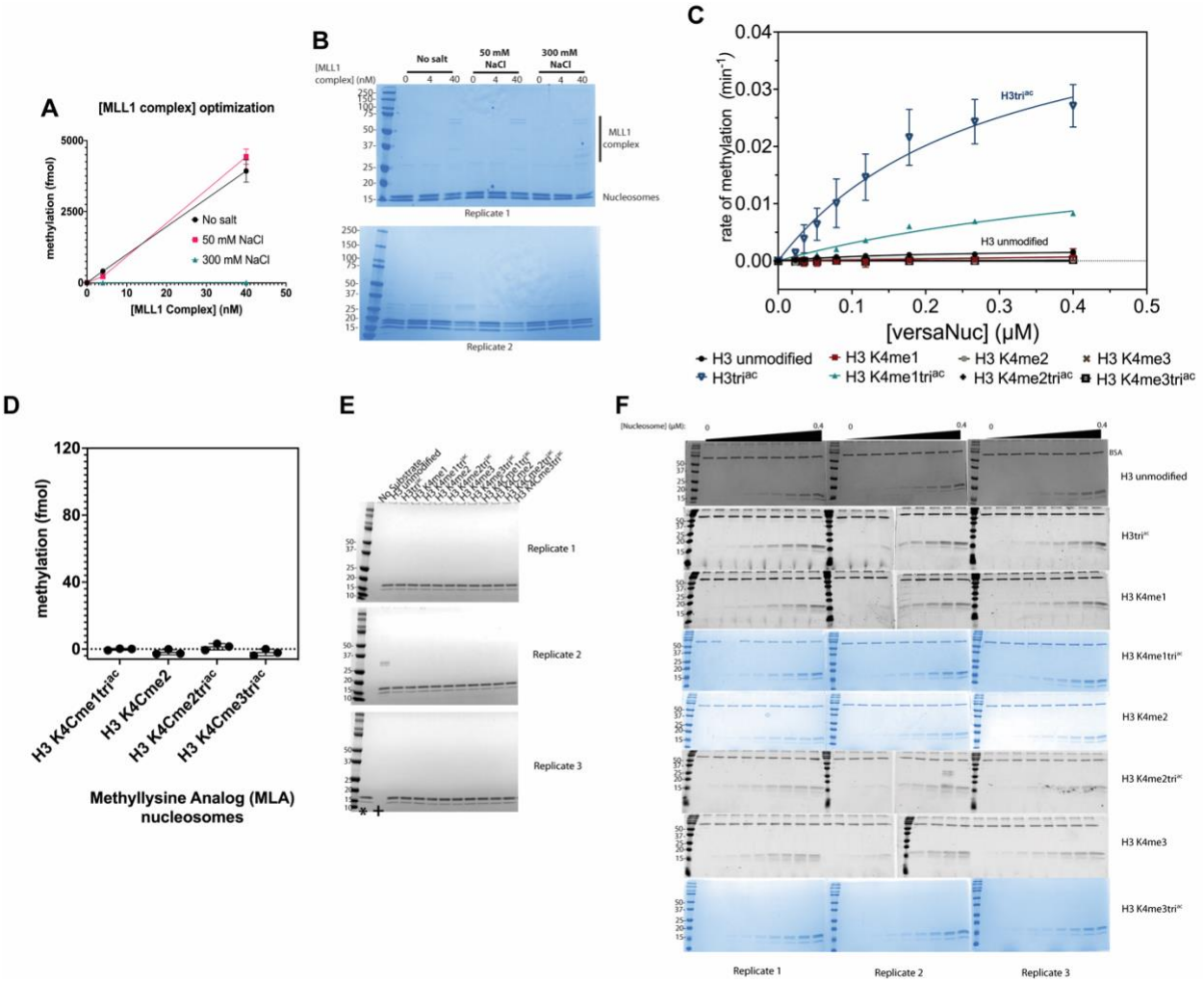

Figure S2. Methylation assays with MLL1C and nucleosome substrate. A) MLL1C (see **Methods**) activity on 2 μg chicken oligonucleosome was 2D-titration tested by enzyme [0, 4 and 40 nM] and salt [0, 50 and 300 mM NaCl] in the presence of [*methyl*-^{3}H]-SAM donor. Methylation (in fmol) is graphed as a function of [MLL1C]. N=2 and error bars are S.D. **B)** Replicate SDS-PAGE Coomassie-stained gels for methylation data from panel **A**. Resolved subunits of MLL1C and nucleosomes are indicated. **C)** Steady-state kinetic data for MLL1C activity with nucleosome substrates as shown in **Figure 2B** but fit to the Michaelis-Menten equation. **D)** Endpoint

497 methylation activity of MLL1C (4 nM) with MLA (methyl-lysine analog) nucleosome substrates
498 (100 nM) in triplicate; error bars are S.D. **E)** Replicate SDS-PAGE Coomassie-stained gels for
499 methylation data from panel **D**; Lanes marked with "*" and "+" in the Replicate 3 gel are switched.
500 **F)** Replicate SDS-PAGE Coomassie-stained gels for methylation data from **Figure 2B** and **Figure**
501 **S2C**. 0.5 μg BSA was loaded in each lane (except for the H3K4me3tri^{ac} reactions) after the
502 reaction was quenched as a lane marker. All data were plotted using GraphPad Prism 9.0.
503

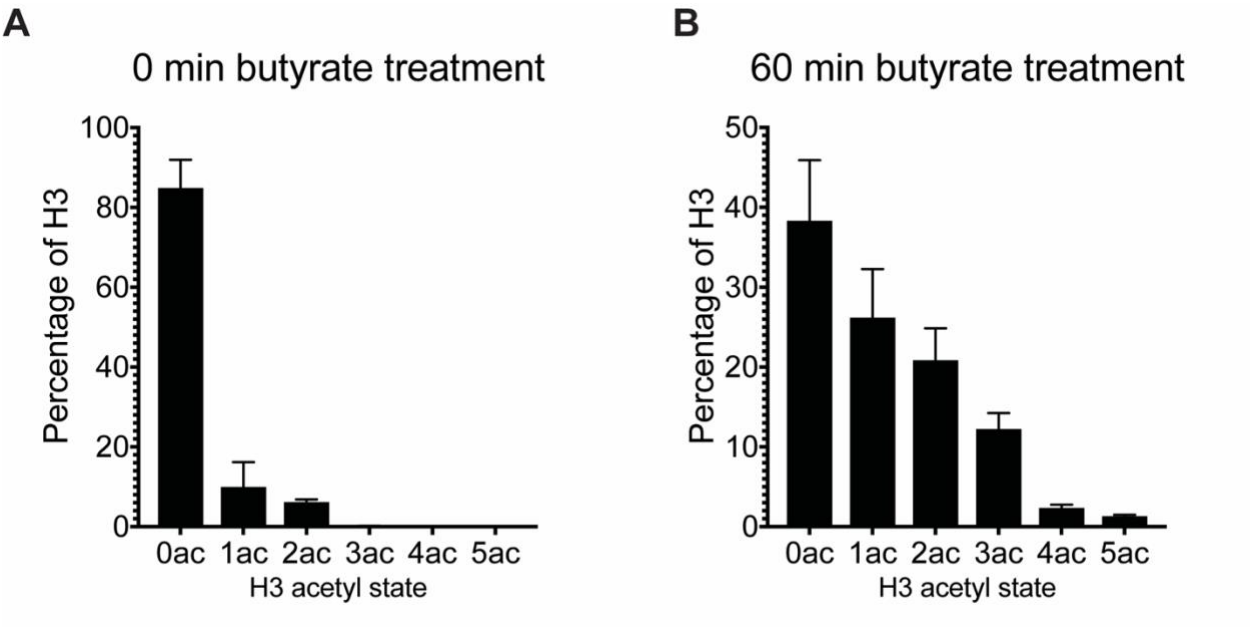

504

505 **Figure S3. H3 acetylation states with sodium butyrate treatment**. **A & B)** Each acetyl group
506 of acid-extracted H3 from 0ac to 5ac is represented as a percent of total H3 before / after 60-
507 minute treatment of asynchronous MCF-7 cells with 5 mM sodium butyrate; n=3 and error bars
508 are S.E.M

509
510
511
512
513
514

TABLE S1: Steady-state Michaelis-Menten kinetic parameters

Substrate	K_M (μM)	k_{cat} (min^{-1})	R^2
H3 unmodified	0.19 ± 0.06	0.0022 ± 0.0003	0.8791
H3 K9/14/18Ac	0.29 ± 0.09	0.0494 ± 0.0085	0.9034
H3 K4me1	n.d. [a]	n.d. [a]	0.1961
H3 K4me1 K9/14/18Ac	0.61 ± 0.16	0.0221 ± 0.0044	0.9646
H3 K4me2	n.d. [a]	n.d. [a]	-0.2004
H3 K4me2 K9/14/18Ac	0.08 ± 0.04	0.0007 ± 0.0001	0.7028
H3 K4me3	n.d. [a]	n.d. [a]	n.d. [a]
H3 K4me3 K9/14/18Ac	n.d. [a]	n.d. [a]	n.d. [a]

[a] = methylation signal observed was indistinguishable from background and thus kinetic parameters could not be determined.

TABLE S2. Mass Spectrometric data for H3K4 methylation and H3 acetylation in asynchronous MCF-7 cells as a function of butyrate treatment. (See Excel file)

REFERENCES

Garcia BA, Pesavento JJ, Mizzen CA, Kelleher NL. 2007. Pervasive combinatorial modification of histone H3 in human cells. *Nature Methods* **4**:487–489. doi:10.1038/nmeth1052

Ghoneim M, Fuchs HA, Musselman CA. 2021. Histone Tail Conformations: A Fuzzy Affair with DNA. *Trends in Biochemical Sciences*. doi:10.1016/j.tibs.2020.12.012

Goswami J, MacArthur T, Bailey K, Spears G, Kozar RA, Auton M, Dong JF, Key NS, Heller S, Loomis E, Hall NW, Johnstone AL, Park MS. 2021. Neutrophil Extracellular Trap Formation and Syndecan-1 Shedding Are Increased After Trauma. *Shock* **56**:433–439. doi:10.1097/SHK.0000000000001741

Greer EL, Beese-Sims SE, Brookes E, Spadafora R, Zhu Y, Rothbart SB, Aristizábal-Corrales D, Chen S, Badeaux AI, Jin Q, Wang W, Strahl BD, Colaiácovo MP, Shi Y. 2014. A Histone Methylation Network Regulates Transgenerational Epigenetic Memory in C. elegans. *Cell Reports* **7**:113–126. doi:10.1016/J.CELREP.2014.02.044

Holt M v, Wang T, Young N. 2021. Expeditious Extraction of Histones from Limited Cells or Tissue Samples and Quantitative Top-Down Proteomic Analysis. *Curr Protoc* **1**. doi:10.1002/CPZ1.26

Holt M v., Wang T, Young NL. 2019. High-Throughput Quantitative Top-Down Proteomics: Histone H4. *J Am Soc Mass Spectrom* **30**:2548–2560. doi:10.1007/s13361-019-02350-z

Hörmanseder E, Simeone A, Allen GE, Bradshaw CR, Figlmüller M, Gurdon J, Jullien J. 2017. H3K4 Methylation-Dependent Memory of Somatic Cell Identity Inhibits Reprogramming and Development of Nuclear Transfer Embryos. *Cell Stem Cell* **21**:135-143.e6. doi:10.1016/J.STEM.2017.03.003

Jain K, Fraser CS, Marunde MR, Parker MM, Sagum C, Burg JM, Hall N, Popova IK, Rodriguez KL, Vaidya A, Krajewski K, Keogh M-C, Bedford MT, Strahl BD. 2020. Characterization of the plant homeodomain (PHD) reader family for their histone tail interactions. *Epigenetics & Chromatin 2020 13:1* **13**:1–11. doi:10.1186/S13072-020-0328-Z

Jenuwein T, Allis CD. 2001. Translating the Histone Code. *Science (1979)* **293**:1074–1080. doi:10.1126/science.1063127

Lee YT, Ayoub A, Park SH, Sha L, Xu J, Mao F, Zheng W, Zhang Y, Cho US, Dou Y. 2021. Mechanism for DPY30 and ASH2L intrinsically disordered regions to modulate the MLL/SET1 activity on chromatin. *Nature Communications* **12**. doi:10.1038/s41467-021-23268-9

Marunde MR, Fuchs HA, Burg JM, Popova IK, Vaidya A, Hall NW, Meiners MJ, Watson R, Howard SA, Novitzky K, McAnarney E, Cheek MA, Sun Z-W, Venters BJ, Keogh M-C, Musselman CA. 2022a. Nucleosome conformation dictates the histone code. *bioRxiv* 2022.02.21.481373. doi:10.1101/2022.02.21.481373

Marunde MR, Popova IK, Weinzapfel EN, Keogh M-C. 2022b. The dCypher Approach to Interrogate Chromatin Reader Activity Against Posttranslational Modification-Defined Histone Peptides and Nucleosomes 231–255. doi:10.1007/978-1-0716-2140-0_13

Morgan MAJ, Popova IK, Vaidya A, Burg JM, Marunde MR, Rendleman EJ, Dumar ZJ, Watson R, Meiners MJ, Howard SA, Khalatyan N, Vaughan RM, Rothbart SB, Keogh M-C, Shilatifard A. 2021. A trivalent nucleosome interaction by PHIP/BRWD2 is disrupted in neurodevelopmental disorders and cancer. *Genes Dev*. doi:10.1101/GAD.348766.121

Morris SA, Rao B, Garcia BA, Hake SB, Diaz RL, Shabanowitz J, Hunt DF, Allis CD, Lieb JD, Strahl BD. 2007. Identification of histone H3 lysine 36 acetylation as a highly conserved histone modification. *Journal of Biological Chemistry* **282**:7632–7640. doi:10.1074/jbc.M607909200

Morrison EA, Bowerman S, Sylvers KL, Wereszczynski J, Musselman CA. 2018. The conformation of the histone H3 tail inhibits association of the BPTF PHD finger with the nucleosome. *Elife* **7**. doi:10.7554/eLife.31481

574 Muramoto T, Müller I, Thomas G, Melvin A, Chubb JR. 2010. Methylation of H3K4 Is Required
575 for Inheritance of Active Transcriptional States. *Current Biology* **20**:397–406.
576 doi:10.1016/J.CUB.2010.01.017
577 Musselman CA, Lalonde M-E, Côté J, Kutateladze TG. 2012. Perceiving the epigenetic
578 landscape through histone readers. *Nature Structural & Molecular Biology 2012 19:12*
579 **19**:1218–1227. doi:10.1038/nsmb.2436
580 Namitz KEW, Tan S, Cosgrove MS. 2019. Hierarchical assembly of the MLL1 core complex
581 within a biomolecular condensate regulates H3K4 methylation. *bioRxiv*.
582 doi:10.1101/870667
583 Nautiyal K, Kuroda Y. 2018. A SEP tag enhances the expression, solubility and yield of
584 recombinant TEV protease without altering its activity. *New Biotechnology* **42**:77–84.
585 doi:10.1016/j.nbt.2018.02.006
586 Ng HH, Robert F, Young RA, Struhl K. 2003. Targeted Recruitment of Set1 Histone Methylase
587 by Elongating Pol II Provides a Localized Mark and Memory of Recent Transcriptional
588 Activity. *Molecular Cell* **11**:709–719. doi:10.1016/S1097-2765(03)00092-3
589 Nightingale KP, Gendreizig S, White DA, Bradbury C, Hollfelder F, Turner BM. 2007. Cross-talk
590 between Histone Modifications in Response to Histone Deacetylase Inhibitors: MLL4
591 LINKS HISTONE H3 ACETYLATION AND HISTONE H3K4 METHYLATION. *Journal of*
592 *Biological Chemistry* **282**:4408–4416. doi:10.1074/JBC.M606773200
593 Park SH, Ayoub A, Lee YT, Xu J, Kim H, Zheng W, Zhang B, Sha L, An S, Zhang Y, Cianfrocco
594 MA, Su M, Dou Y, Cho US. 2019. Cryo-EM structure of the human MLL1 core complex
595 bound to the nucleosome. *Nature Communications* **10**. doi:10.1038/s41467-019-13550-2
596 Patel A, Dharmarajan V, Vought VE, Cosgrove MS. 2009. On the mechanism of multiple lysine
597 methylation by the human mixed lineage leukemia protein-1 (MLL1) core complex. *Journal*
598 *of Biological Chemistry* **284**:24242–24256. doi:10.1074/jbc.M109.014498
599 Patel A, Vought VE, Dharmarajan V, Cosgrove MS. 2011. A Novel Non-SET Domain Multi-
600 subunit Methyltransferase Required for Sequential Nucleosomal Histone H3 Methylation by
601 the Mixed Lineage Leukemia Protein-1 (MLL1) Core Complex *. *Journal of Biological*
602 *Chemistry* **286**:3359–3369. doi:10.1074/jbc.M110.174524
603 Peach SE, Rudomin EL, Udeshi ND, Carr SA, Jaffe JD. 2012. Quantitative Assessment of
604 Chromatin Immunoprecipitation Grade Antibodies Directed against Histone Modifications
605 Reveals Patterns of Co-occurring Marks on Histone Protein Molecules. *Molecular &*
606 *Cellular Proteomics* **11**:128–137. doi:10.1074/MCP.M111.015941
607 Rao RC, Dou Y. 2015. Hijacked in cancer: The KMT2 (MLL) family of methyltransferases.
608 *Nature Reviews Cancer*. doi:10.1038/nrc3929
609 Rossetto D, Avvakumov N, Côté J. 2012. Histone phosphorylation. *Epigenetics* **7**:1098–1108.
610 doi:10.4161/epi.21975
611 Santos-Rosa H, Schneider R, Bannister AJ, Sherriff J, Bernstein BE, Emre NCT, Schreiber SL,
612 Mellor J, Kouzarides T. 2002. Active genes are tri-methylated at K4 of histone H3. *Nature*
613 *2002 419:6905* **419**:407–411. doi:10.1038/nature01080
614 Sha L, Ayoub A, Cho US, Dou Y. 2020. Insights on the regulation of the MLL/SET1 family
615 histone methyltransferases. *Biochimica et Biophysica Acta - Gene Regulatory*
616 *Mechanisms*. doi:10.1016/j.bbagrm.2020.194561
617 Shinsky SA, Monteith KE, Viggiano S, Cosgrove MS. 2015. Biochemical reconstitution and
618 phylogenetic comparison of human SET1 family core complexes involved in histone
619 methylation. *Journal of Biological Chemistry* **290**:6361–6375. doi:10.1074/jbc.M114.627646
620 Simon MD, Shokat KM. 2012. A Method to Site-Specifically Incorporate Methyl-Lysine
621 Analogues into Recombinant Proteins. *Methods in Enzymology* **512**:57–69.
622 doi:10.1016/B978-0-12-391940-3.00003-2
623 Smith LM, Kelleher NL. 2013. Proteoform: a single term describing protein complexity. *Nature*
624 *Methods 2013 10:3* **10**:186–187. doi:10.1038/nmeth.2369

Strahl BD, Allis CD. 2000. The language of covalent histone modifications. *Nature* **403**:41–45. doi:10.1038/47412

Strahl BD, Ohba R, Cook RG, Allis CD. 1999. Methylation of histone H3 at lysine 4 is highly conserved and correlates with transcriptionally active nuclei in Tetrahymena. *Proceedings of the National Academy of Sciences* **96**:14967–14972. doi:10.1073/PNAS.96.26.14967

Strelow JM, Xiao M, Cavitt RN, Fite NC, Margolis BJ, Park KJ. 2016. The Use of Nucleosome Substrates Improves Binding of SAM Analogs to SETD8. *Journal of Biomolecular Screening* **21**:786–794. doi:10.1177/1087057116656596

Stützer A, Liokatis S, Kiesel A, Schwarzer D, Sprangers R, Söding J, Selenko P, Fischle W. 2016. Modulations of DNA Contacts by Linker Histones and Post-translational Modifications Determine the Mobility and Modifiability of Nucleosomal H3 Tails. *Molecular Cell* **61**:247–259. doi:10.1016/J.MOLCEL.2015.12.015/ATTACHMENT/48EB5ADD-404B-4984-923B-7C6FC2E26120/MMC1.PDF

Su Z, Denu JM. 2016. Reading the Combinatorial Histone Language. *ACS Chemical Biology* **11**:564–574. doi:10.1021/acschembio.5b00864

Tan S, Kern RC, Selleck W. 2005. The pST44 polycistronic expression system for producing protein complexes in Escherichia coli. *Protein Expression and Purification* **40**:385–395. doi:10.1016/j.pep.2004.12.002

Taverna SD, Ueberheide BM, Liu Y, Tackett AJ, Dias RL, Shabanowitz J, Chait BT, Hunt DF, Allis CD. 2007. Long-distance combinatorial linkage between methylation and acetylation on histone H3 N termini. *Proc Natl Acad Sci U S A* **104**:2086–2091. doi:10.1073/pnas.0610993104

Taylor BC, Young NL. 2021. Combinations of histone post-translational modifications. *Biochemical Journal* **478**:511–532. doi:10.1042/BCJ20200170

Trush V v., Feller C, Li ASM, Allali-Hassani A, Szewczyk MM, Chau I, Eram MS, Jiang B, Luu R, Zhang F, Barsyte-Lovejoy D, Aebersold R, Arrowsmith CH, Vedadi M. 2022. Enzymatic nucleosome acetylation selectively affects activity of histone methyltransferases in vitro. *Biochimica et Biophysica Acta (BBA) - Gene Regulatory Mechanisms* **1865**:194845. doi:10.1016/J.BBAGRM.2022.194845

Usher ET, Namitz KEW, Cosgrove MS, Showalter SA. 2021. Probing multiple enzymatic methylation events in real time with NMR spectroscopy. *Biophysical Journal* **120**:4710–4721. doi:10.1016/J.BPJ.2021.09.034

Vaughan RM, Kupai A, Rothbart SB. 2021. Chromatin Regulation through Ubiquitin and Ubiquitin-like Histone Modifications. *Trends in Biochemical Sciences*. doi:10.1016/j.tibs.2020.11.005

Weinberg DN, Papillon-Cavanagh S, Chen H, Yue Y, Chen X, Rajagopalan KN, Horth C, McGuire JT, Xu X, Nikbakht H, Lemiesz AE, Marchione DM, Marunde MR, Meiners MJ, Cheek MA, Keogh M-C, Bareke E, Djedid A, Harutyunyan AS, Jabado N, Garcia BA, Li H, Allis CD, Majewski J, Lu C. 2019. The histone mark H3K36me2 recruits DNMT3A and shapes the intergenic DNA methylation landscape. *Nature* **573**:281–286. doi:10.1038/s41586-019-1534-3

Weinberg DN, Rosenbaum P, Chen X, Barrows D, Horth C, Marunde MR, Popova IK, Gillespie ZB, Keogh MC, Lu C, Majewski J, Allis CD. 2021. Two competing mechanisms of DNMT3A recruitment regulate the dynamics of de novo DNA methylation at PRC1-targeted CpG islands. *Nature Genetics* **53**:794–800. doi:10.1038/s41588-021-00856-5

Weiss JN. 1997. The Hill equation revisited: uses and misuses. *The FASEB journal : official publication of the Federation of American Societies for Experimental Biology* **11**:835–841. doi:0892-6638/97/0011

Worden EJ, Wolberger C. 2019. Activation and regulation of H2B-Ubiquitin-dependent histone methyltransferases. *Current Opinion in Structural Biology* **59**:98–106. doi:10.1016/J.SBI.2019.05.009

Wozniak G, Strahl B. 2014. Hitting the “mark”: interpreting lysine methylation in the context of active transcription. *Biochim Biophys Acta* **1839**:1353–1361. doi:10.1016/J.BBAGRM.2014.03.002

Xue H, Yao T, Cao M, Zhu G, Li Y, Yuan G, Chen Y, Lei M, Huang J. 2019. Structural basis of nucleosome recognition and modification by MLL methyltransferases. *Nature* **573**:445–449. doi:10.1038/s41586-019-1528-1

Young NL, DiMaggio PA, Garcia BA. 2010. The significance, development and progress of high-throughput combinatorial histone code analysis. *Cellular and Molecular Life Sciences 2010 67:23* **67**:3983–4000. doi:10.1007/S00018-010-0475-7

Young NL, DiMaggio PA, Plazas-Mayorca MD, Baliban RC, Floudas CA, Garcia BA. 2009. High throughput characterization of combinatorial histone codes. *Molecular and Cellular Proteomics* **8**:2266–2284. doi:10.1074/mcp.M900238-MCP200